Renewable Energy 220 (2024) 119683

Contents lists available at ScienceDirect

Renewable Energy

journal homepage: www.elsevier.com/locate/renene

Assessing the Tidal Stream Resource for energy extraction in The Netherlands

Matias Alday *, George Lavidas

Marine Renewable Energies Lab., Offshore Engineering group, Department of Hydraulic Engineering, Delft University of Technology, Stevinweg 1, Delft, 2628 CN, The Netherlands

ARTICLE INFO

Keywords:
Tidal stream resource
Thetis
Unstructured mesh
North Sea

ABSTRACT

In order to accelerate the transition from carbon fuels to renewable energy sources, it is essential to extend our knowledge of the resources' availability to further improve or adjust the design of extraction devices. In the present paper, a first characterization of the tidal stream resource along the coast of The Netherlands is performed using a high-resolution unstructured grid implementation of the Thetis model. Extensive validation of the sea surface elevations was done by comparing with existing networks of tide gauges in the North Sea. The simulations from this study show that the highest tidal current intensities are generated mainly at Den Helder and Oost Vlieland, reaching values >1.5 m s^{-1} and power density estimates that are most frequently close to 300 W m^{-2} and that can reach values ≥ 900 W m^{-2}. Given the relatively reduced depths where these "hot spots" are found, most existing stream turbines will require further development to operate. Nevertheless, the existence of higher current intensities zones, along a commonly considered "low energy" coast, opens the door to include the tidal stream resource in near future plans to diversify the energy supply in The Netherlands.

1. Introduction

The task to reduce the high-dependency of the energy supply from carbon fuels is a commitment and a challenge undertaken by many governments. This venture forces us to look for different (and potentially complementary) sources for energy generation, and to further adapt already existing extraction devices to environmental conditions once considered not suitable. Unlike wind, one of the key features that makes the tidal energy resource attractive for electricity generation, is its predictability. Although there would be a locally intermittent production, characteristic of a given site's tidal cycle, this effect can be mitigated with a carefully designed layout of energy converters taking advantage of the tidal phase lag along the coast [e.g.; 1]. The stream profiles also depend on local conditions, but since astronomical tides are stochastic the mean and maximum velocities will not deviate much at a specific site. This element can assist in the scaling and adaptability of tidal turbines to increase their efficiency and utilization rates. Despite the "early development stage" of the extraction technology for tidal stream, it is agreed that it holds a large potential. Consequently, there has been an increasing amount of studies aimed to better understand the resource and production possibilities: Neill et al. [2], Vogel et al. [3], Mejia-Olivares et al. [4], Guillou et al. [5], Guerra et al. [6], Orhan et al. [7].

While high tidal ranges are typically desired for harnessing tidal power with barrages [e.g.; 8,9], sites without such highly energetic potential for energy extraction can still present interesting conditions for stream turbines. In areas of relatively shallow water depths and complex coastlines configurations, bathymetry features become more important due to the interaction of the tidal wave with the local topography. They can significantly modify the hydrodynamic field, potentially inducing areas of high velocities [10]. Thus, these areas can be developed even when tidal elevation's amplitude is not necessarily "extreme" as found in some locations of the English Channel or in the UK. The identification and characterization of the tidal stream resource within these high velocities areas, along the coast of The Netherlands, is one of the main subjects of the present paper.

The scarce availability of studies dedicated to the characterization of the Dutch stream tidal resource probably comes from its well know "low amplitudes". Most studies analyzing tidal characteristics of the Dutch coast have typically focused on the role of this forcing in the context of deltas dynamics, tides-storm interactions and their effect on sediment transport. These represent important elements for the maintenance of shipping routes and the stability of coastal structures [e.g.; 11–13]. In recent years, and in the context of climate change effects, more efforts have been put into analyzing potential changes of the tidal regime in bays and inlets [e.g.; 14,15]. There have been a few particular projects developed within Dutch inlets, taking advantage of modifications introduced by storm surge barriers [like the Tocardo Tidal Power project; 16]. But outside some scarce studies locally detailed, like de Fockert et al. [17], the overall stream energy potential has never been properly analyzed.

* Corresponding author.
E-mail addresses: M.F.AldayGonzalez@tudelft.nl (M. Alday), G.Lavidas@tudelft.nl (G. Lavidas).

https://doi.org/10.1016/j.renene.2023.119683
Received 6 February 2023; Received in revised form 14 October 2023; Accepted 16 November 2023
Available online 18 November 2023

The Netherlands has progressively increased its interest in alternative sources for energy generation. Outside the more developed and studied offshore wind sector [18–20], tidal stream is regarded as an interesting option for diversification. Currently, there are several data from in situ measurements of sea level elevations in The North Sea, and output from a few existing global and regional tide models [e.g.; 21–23]. Nevertheless, there is a clear necessity for a high resolution dataset to analyze the characteristics of the tidal stream along the Dutch coast.

With the aim to identify the presence of areas with potential for tidal stream energy conversion, a first effort to characterize the sea surface elevation and velocities pattern induced by astronomical tides along the Dutch coast is performed in this study. A complete analysis of the tidal stream potential is developed based on a 1 year half-hourly tide dataset, obtained from a high resolution hydrodynamic model implemented for this purpose. Additionally, to improve the characterization of current intensities or stream power densities distributions, an area-selecting approach, including minimum depth operation restrictions, is proposed. Based on the overall assessment and the latter suggested method, a selection of locations with energy extraction potential is performed. Due to the nature of the resource, and according to international guidelines our approach satisfies the standard protocols [equimar; 24].

The content of this paper is structured as follows: The introduction to the study in Section 1. In Section 2, the hydrodynamic model implementation, model performance parameters, and general characteristics of tides within the North Sea are detailed. Then, in Section 3, the validation and estimation of the model accuracy, and the characterization of the tidal stream along the Dutch coast are presented, with a discussion on the findings from this study. Finally, conclusions are included in Section 4.

2. Materials and methods

2.1. The thetis model

Thetis [25] is an open source python-based ocean and coastal modeling suit, that works with the Firedrake finite element framework [26] and the Portable, Extensible Toolkit for Scientific Computation [PETSc; 27,28] to solve Partial Differential Equations (PDE) systems.

Astronomical tides are long barotropic waves, given their nature and the purpose of the present study, it is suitable to represent the induced motions in the water column as 2-dimensional, neglecting the vertical velocities component. In our implementation of Thetis the Nonlinear Shallow Water Equations (NLSWE) are solved over finite elements of an unstructured grid (mesh). The system is solved in space and time respectively with a CG-type [29] and a 2-stage 2nd order L-stable Diagonally Implicit Runge Kutta method [DIRK22; 30] implicit method.

The depth averaged shallow water equations as implemented in Thetis are described as follows:

$$\frac{\partial \eta}{\partial t} + \nabla \cdot (H\bar{u}) = 0 \tag{1}$$

$$\frac{\partial \bar{u}}{\partial t} + \bar{u} \cdot \nabla \bar{u} + f e_z \wedge \bar{u} + g\nabla\eta + \nabla\left(\frac{p_a}{\rho_0}\right) + g\frac{1}{H}\int_{-h}^{\eta} \nabla r dz = \nabla \cdot \left(\nu_h(\nabla\bar{u} + (\nabla\bar{u})^T)\right) + \frac{\nu_h \nabla(H)}{H} \cdot (\nabla\bar{u} + (\nabla\bar{u})^T) \tag{2}$$

with

$$r = \frac{1}{\rho_0}\int_z^{\eta} \rho' d\zeta \tag{3}$$

$$f = 2\Omega sin(\varphi) \tag{4}$$

and

$$H = \eta + h \tag{5}$$

In Eqs. (1) to (5) g is the acceleration of gravity (taken as 9.81 m s^{-1}), f is the Coriolis frequency, with $\Omega = 7.2921 \times 10^5$ rad s^{-1} the rotation frequency of the Earth and φ the latitude. The water density as a function of temperature, salinity and pressure is expressed as $\rho = \rho(T, S, p)' + \rho_0$, where ρ_0 is a constant reference water density (taken as 1023.6 kg m^{-3}). Then, p_a is the atmospheric pressure at the free surface, ν_h is the horizontal viscosity (set to 0 by default) and h the local mean depth.

The state variables are the water elevation η and the depth averaged velocity vector $\bar{u}$. Eq. (1) is the non-conservative form of the free surface, Eq. (2) is the expression for the non-conservative momentum, where Eq. (4) denotes the baroclinic head. In particular for our application with purely barotropic components, Eq. (4) and the internal pressure gradient are omitted. Finally, the total water column depth is given by Eq. (5).

It should be noticed that no external pressure forcing is included, since only the effect of astronomical tides are considered. Thus, the fifth term from the left-hand side in Eq. (2) is zero ($\nabla(p_a/\rho_0) = 0$). This simplification implies that changes in the sea surface elevations and current patterns induced by strong atmospheric events, like storm surges, are not represented. Furthermore, the effect of surface drag caused by the wind is not considered, which implies that potential changes in sea surface elevations due to wind setup is also not simulated. Although, given its characteristics, it is thought that this latter effect might be of importance in mainly shallow areas close to the coast.

Even though the implicit time solving scheme is unconditionally stable, a maximum time step of 360 s was defined based on CFL stability conditions for explicit numerical methods [31]. This is done to prevent the simulation of unrealistic levels and/or current intensities values in those regions of the modeled domain with high resolution. In the same line, a minimum depth threshold of 7 m is applied in the model, which means that shallower depths are internally set to this minimum depth in Thetis. Since wet and dry effects are not considered in our simulations, the minimum imposed depth helps to ensure the model stability in those shallow areas with tidal amplitudes of the same order. Finally, with a sensitivity analysis (not shown), an ad hoc homogeneous Manning friction coefficient of 0.02 $m^{1/3}s^{-1}$ was set for the complete domain. The sensitivity analysis included the comparison of 1-month simulations with elevations from tide gauges data at several locations within Dutch waters (see Fig. 3), in particular for July 2016. The selected Manning value corresponds to the one that provided the best model performance when compared to most of the local measurements. July was selected since the influence of strong atmospheric gradients or energetic sea states is very low in the North Sea. Hence, the in situ records are less "noisy", and thus more reliable for performing a direct comparison with the modeled elevations or to use the spectral analysis (e.g.; Fig. 7). One of the main drawbacks of using a homogeneous bottom friction value, is that it can introduce undesired effects in the propagation of the resulting tidal wave, mainly slight phase and amplitude changes. This approach should be re-visited/improved in further efforts to help reduce the spatial distribution of random errors [e.g.; 32].

Output of the depth averaged velocities components u and v, and water elevation is requested each 30 min.

2.2. Mesh construction

The two-dimensional unstructured grid was generated using the qmesh mesh generator [33], integrating coastlines from OpenStreetMaps [from hereon OSM; 34] and bathymetry data from the EMODnet digital elevation model [version 2020; 35] with a gridded resolution of ~115 m. Before the mesh generation, the variable resolution from OSM polygons was homogenized along the Dutch coast at a maximum resolution of ~500 m applying decreasing resolution along the English Channel, the UK and the Atlantic coast of Europe. All small islands outside the area of interest and in deep water depths were not considered to optimize modeling time and CPU usage.

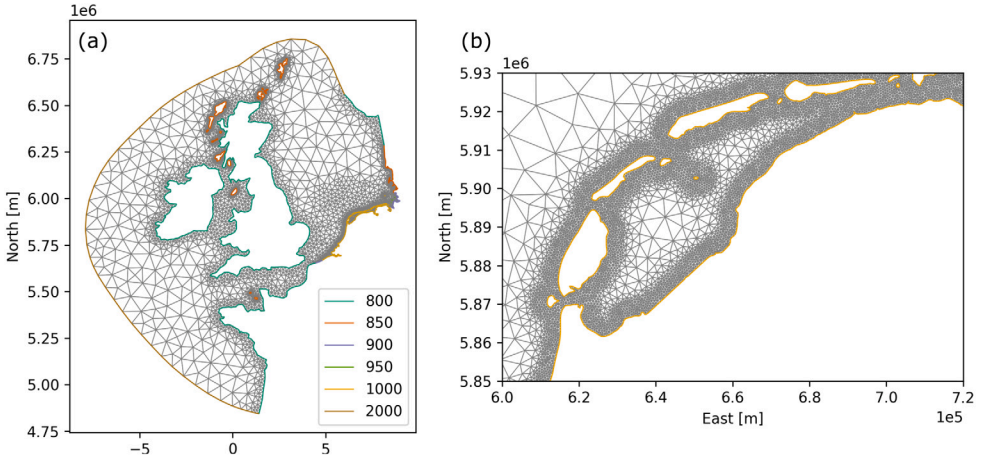

Fig. 1. (a) Mesh elements distribution in full domain (b) Mesh elements detail along part of the Dutch coast. ID = 2000 is the open ocean boundary where boundary conditions are prescribed. ID = 1000 is the Dutch coast boundary with maximum resolution. ID's 950 to 800 are used to help reducing mesh elements resolution towards the open boundary.

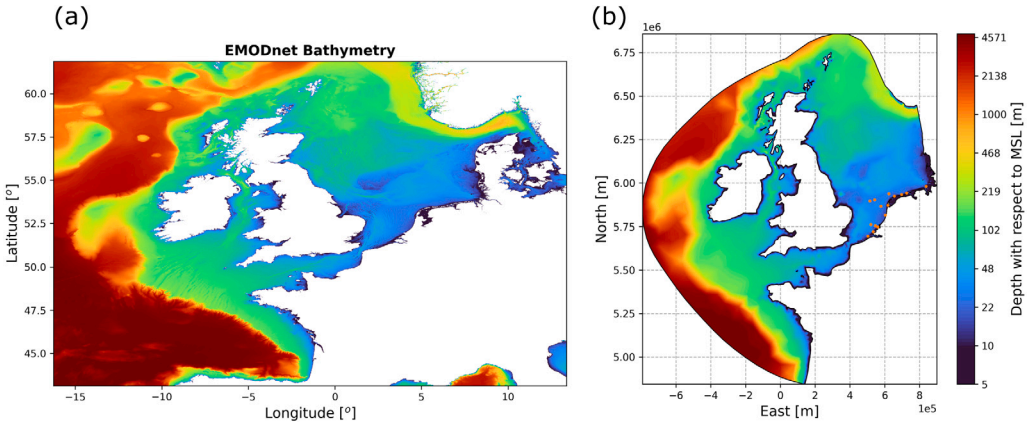

Fig. 2. (a) EMODnet bathymetry (original projection). (b) Bathymetry interpolated into mesh nodes. Orange points in (b) show the location of the tide gauges used for validation.

Both, bathymetry and coastlines data were re-projected from geographical coordinates to WGS84, UTM zone 31 North. Additionally, bathymetry's vertical datum was transformed from Lowest Astronomical Tide (LAT) to Mean Sea Level (MSL) with the M_2, S_2, N_2, K_1 and O_1 tidal harmonics' amplitudes from the Ifremer's Tidal Atlas [22] using the following approximation:

$$\mathrm{LAT}_{(x,y)} = \quad Zo_{(x,y)} - \sum(A_{i(x,y)}) \tag{6}$$

where $\mathrm{LAT}_{(x,y)}$ is the estimated LAT datum at a given location (x,y), Z_o the local mean sea level in m, and $\mathrm{A}_{i(x,y)}$ is the amplitude in m from the ith considered harmonic for datum correction.

The modeled domain is extended to deep waters off the European coastal shelf in most of its extension along the North Atlantic. This is done to facilitate numerical stability and allow the tidal waves' interaction with the main bathymetric features as it propagates towards the Dutch coast. To control the mesh elements size distribution, mainly 2 restrictions or metrics where taken into account. First, a minimum element size related to wave propagation celerity ($C = \sqrt{gH}$) in shallow waters, which is proportional to the local depth (H), considering that $N = 3$ mesh elements are required to capture the minimum tidal wave length as proposed in Lambrechts et al. [36]. The second metric is related to the minimum element side length desired at identified boundaries (e.g. open boundaries, continental or islands coastlines) and how they grow as function to the distance from each given boundary. A total of 6 boundaries IDs where defined to progressively increase the mesh elements' size towards the open boundary in deep waters (ID = 2000) and still preserve relevant coastlines and bathymetry features. Along the Dutch coast (boundary ID = 1000) we defined a minimum element side length of 500 m, this restriction is only relaxed 4 km off the shore to ensure a high resolution band along the area of interest (Fig. 1).

Once the mesh is generated, the input bathymetry is interpolated into the mesh's nodes in Thetis, in this case using bi-linear interpolation (see Fig. 2).

2.3. Tidal forcing

The model is forced with tidal levels at the open ocean boundary (Fig. 1a). The tidal levels are generated based on the harmonics (amplitudes and phases) taken from the Oregon State University (OSU) TPXO global barotropic tide model [TPXO9v5a; 21]. A total of 11 harmonics are included: Q_1, O_1, P_1, K_1, N_2, M_2, S_2, K_2, M_3, M_4, and S_1. The amplitudes and phases with originally 1/6° grid resolution are interpolated along the nodes of the open boundary. The placement of the open boundary in deep waters (outside the coastal shelf) was also defined taking into account the small intensities of tidal currents in the area, making it adequate to force just with tidal levels and letting the velocities develop inside the domain.

To force the model, a spin-up time of 15 days was considered with linearly increasing amplitudes until reaching full forcing. After these 15 days, 2 extra days are included applying boundary forcing with full amplitudes before using the modeled output data.

Fig. 3. Location of tide gauges (TG) used for model performance assessment. Map data are taken from ©Google Landsat/Copernicus.

2.4. In situ measurements

To assess the accuracy or the results, a total of 13 locations distributed along the Dutch coast were selected to compare against in-situ measurements. Local tide records are taken from tide gauges (TG) available in the Copernicus Marine Service in Situ TAC (Thematic Assembly Center) platform [37]. The year 2016 was selected for adjustments and validation due to the large amount of simultaneous data available at different locations. The location of the selected tide gauges is presented in Fig. 3.

2.5. Model performance indicators

The following performance parameters are used to assess the accuracy of the hindcast:

$$\mathrm{ABIAS} = \frac{1}{N}\sum(|X_{\mathrm{mod}}| - |X_{\mathrm{obs}}|) \tag{7}$$

$$\mathrm{RMSD} = \sqrt{\frac{\sum(X_{\mathrm{mod}} - X_{\mathrm{obs}})^2}{N}} \tag{8}$$

$$\mathrm{NRMSD} = \sqrt{\frac{\sum(X_{\mathrm{mod}} - X_{\mathrm{obs}})^2}{\sum X_{\mathrm{obs}}^2}} \tag{9}$$

$$\mathrm{CORR} = \frac{\sum(X_{\mathrm{mod}} - \overline{X_{\mathrm{mod}}})(X_{\mathrm{obs}} - \overline{X_{\mathrm{obs}}})}{\sqrt{\sum(X_{\mathrm{mod}} - \overline{X_{\mathrm{mod}}})^2}\sqrt{\sum(X_{\mathrm{obs}} - \overline{X_{\mathrm{obs}}})^2}} \tag{10}$$

where ABIAS is the bias of the absolute value of sea surface elevations. RMSD are the Root Mean squared Differences and NRMSD the Normalized Root Mean Squared Differences. Within these expressions X_{mod} are the modeled tidal elevations and X_{obs} the reference value from measurements (tide gauges).

2.6. Tidal stream characterization

To define potential areas of interest for tidal stream energy conversion, first an overall assessment of the current velocities is performed, identifying the mean maximum intensities (see Section 3.2). Then, based on this analysis, the areas along the coast with higher intensities are selected. Once those areas are identified and selected, a more detailed assessment is proposed considering 2 steps. The first step is the definition of a transect crossing through the place where the highest current intensities are developed locally (within each selected area). These transects, aimed to capture spatial variability, consist of a reduced set of points from which the intensities probability density function (PDF) is estimated. Then, to provide a more general characterization per zone, the PDF is computed integrating all mesh nodes contained within a "semi-arbitrary" area. This selected area is defined trying to incorporate all places with high current velocities, not only the "highest" spots or places too far offshore. Additionally a minimum depth filter is considered to exclude very shallow areas where operation of stream turbines might not be possible (see for example Fig. 10). Finally, these 2 latter steps are repeated to compute the PDFs of tidal stream power density (Section 3.3).

The tidal stream power density in W m^{-2} is computed as follows:

$$\left(\frac{P}{A}\right)_{\mathrm{water}} = \frac{1}{2}\rho U^3 \tag{11}$$

where A is the cross-section area (in m^2) of flow intercepted by a tidal energy converter (TEC), ρ is the water density in kg m^{-3}, here taken as 1025 kg m^{-3}, and U is the current intensity in m s^{-1}.

2.7. Tide characteristics in the North Sea

As commonly found in the rest of the European shelf, dominant tides in the North Sea are semidiurnal, where M2 and S2 present the largest contribution to the variance of the sea surface elevation and currents [14,38]. Most of these oscillations enter from the North, between the Shetlands and Scotland, and to a lesser degree from the English Channel. The semidiurnal tides travel counter-clockwise within the North Sea basin as Kelvin waves, developing larger amplitudes along the Dutch north coast, the German Bight and eastern coast of England. The cyclonic progress of these tides have been explained with the solution to the idealized problem of a Kelvin wave reflection in a rectangular rotating basin with uniform depth and width [39]. This approach also provided predictions on the generation of the elevation and current amphidromic points. In fact, Proudman and Doodson [40] identified 3 main amphidromic points: One in the Flemish banks close to the English Channel, a second one in the central region of the North Sea basin, and a third one off the coast of Norway. Resonant conditions of the North Sea basin are close to the spectral band of the main semidiurnal constituents (M2 and S2). This results in local amplification

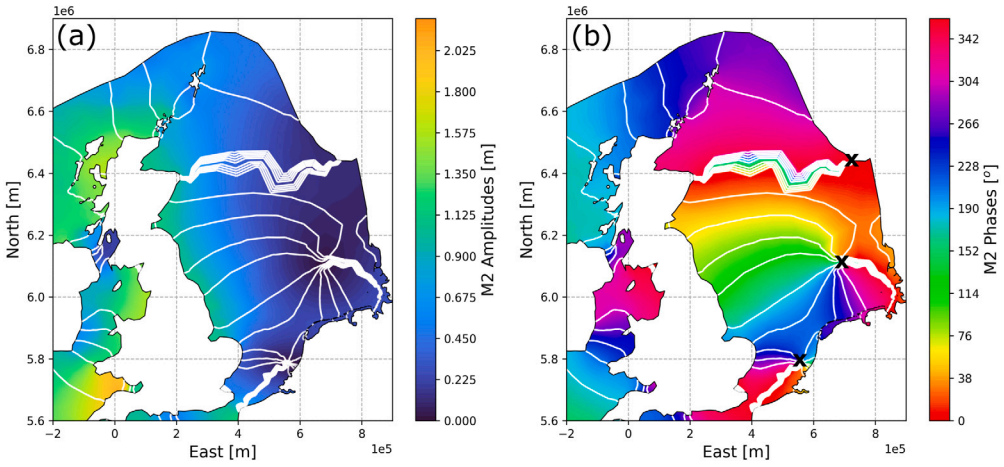

Fig. 4. North Sea M2 constituent characteristics obtained from 1 month simulation. (a) M2 amplitudes in meters with overlaid phases' contours in white. (b) M2 phases in degrees with contours in white and obtained amphidromic points indicated with crosses. Coordinates' projection in UTM, zone 31 U.

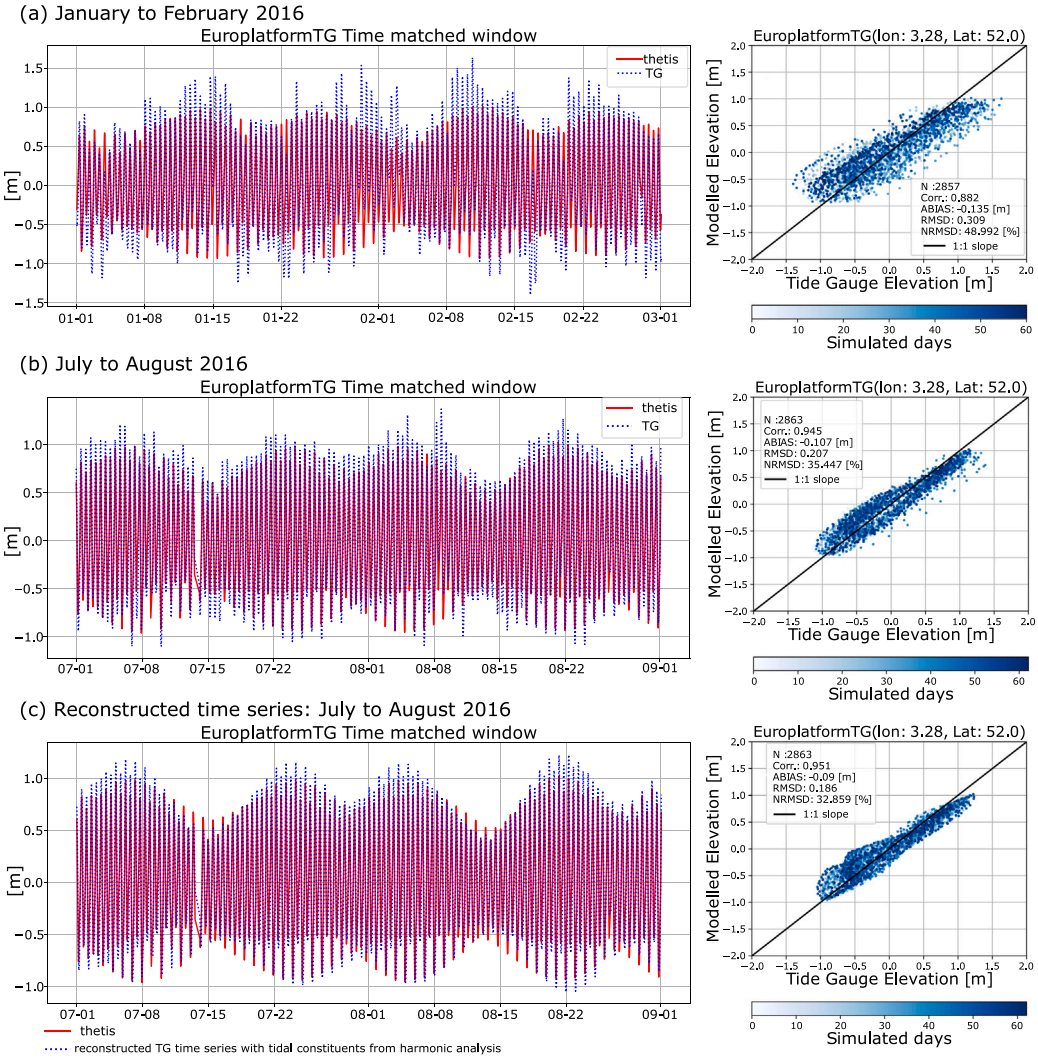

Fig. 5. Model performance briefing at Europlatform TG. Analyzed time windows in year 2016: (a) January to February, (b) July to August, (c) July to August tide gauge reconstructed time series using tidal constituents only. In (b) and (c) there is a gap in the TG data between the 13 and 14 of July.

of the potential tidal range up to 5 m [41–43], although the tidal range can be strongly influenced by bottom friction and local conditions in nearshore areas.

The generation of the aforementioned amphidromic points can be observed in Fig. 4, where we present the M2 characteristics obtained with the proposed model implementation. The point close to Norway

Table 1
Model performance compared to tide gauges. Results computed over time windows of 2 months (in winter and summer) for year 2016. UTM zone for all tide gauges is 31U, with exception of Alte Weser, which is 32U. Performance parameters from Rec. Jul-Aug, correspond to those obtained comparing modeled results with the TG reconstructed time series using only tidal constituents from harmonic analysis.

TG Location Name	Easting [m]	Northing [m]	Time period	ABIAS [m]	RMSD [m]	NRMSD [%]	CORR ($\rho_{Pearson}$)
AlteWeser	442621.49	5968665.37	Jan–Feb	−0.11	0.48	44.04	0.899
			Jul–Aug	−0.085	0.209	20.111	0.983
			Rec. Jul–Aug	−0.031	0.164	16.636	0.987
DenHelder	617519.53	5870366.23	Jan–Feb	−0.770	0.346	57.409	0.819
			Jul–Aug	−0.023	0.161	31.051	0.951
			Rec. Jul–Aug	0.014	0.132	26.875	0.965
Europlatform	519222.13	5761075.22	Jan–Feb	−0.135	0.309	48.992	0.882
			Jul–Aug	−0.107	0.207	35.447	0.945
			Rec. Jul–Aug	−0.09	0.186	32.859	0.951
Haringvliet10	559217.69	5746261.65	Jan–Feb	−0.138	0.343	43.273	0.909
			Jul–Aug	−0.106	0.232	31.45	0.954
			Rec. Jul–Aug	−0.08	0.207	28.711	0.962
Huibertgat	327837.06	5938825.21	Jan–Feb	−0.089	0.397	46.391	0.887
			Jul–Aug	−0.069	0.208	25.676	0.969
			Rec. Jul–Aug	−0.023	0.155	20.003	0.980
IJmondstroompaal	603193.14	5813843.72	Jan–Feb	−0.091	0.308	50.503	0.865
			Jul–Aug	−0.052	0.168	30.316	0.954
			Rec. Jul–Aug	−0.024	0.153	28.414	0.959
K13a	514623.03	5896544.06	Jan–Feb	−0.028	0.266	53.859	0.846
			Jul–Aug	0.022	0.135	30.847	0.956
			Rec. Jul–Aug	−0.033	0.100	23.818	0.979
K141	541749.28	5902378.03	Jan–Feb	−0.030	0.283	56.636	0.828
			Jul–Aug	0.018	0.169	38.022	0.931
			Rec. Jul–Aug	−0.030	0.131	30.984	0.960
L91	623842.61	5936862.57	Jan–Feb	−0.040	0.346	56.459	0.828
			Jul–Aug	−0.001	0.233	41.751	0.912
			Rec. Jul–Aug	−0.016	0.200	37.202	0.934
Oosterschelde11	533215.84	5721108.32	Jan–Feb	−0.186	0.408	38.583	0.932
			Jul–Aug	−0.178	0.338	32.714	0.954
			Rec. Jul–Aug	−0.142	0.316	31.484	0.955
Q11	577233.06	5865101.59	Jan–Feb	−0.04	0.292	58.62	0.812
			Jul–Aug	0.011	0.136	32.279	0.95
			Rec. Jul–Aug	0.041	0.107	27.014	0.971
TerschellingNoordzee	654948.82	5924087.08	Jan–Feb	−0.061	0.375	49.723	0.868
			Jul–Aug	−0.034	0.173	24.642	0.969
			Rec. Jul–Aug	−0.006	0.119	17.690	0.984
Wierumergronden	696173.86	5933859.51	Jan–Feb	−0.078	0.38	47.486	0.88
			Jul–Aug	−0.054	0.199	26.483	0.965
			Rec. Jul–Aug	−0.014	0.141	19.656	0.981

is less well resolved due to the position of the domain boundary. We also note that the position of the southern amphidromic point, close to the English Channel, might be slightly shifted to the east compared to other models [e.g.; 14,22]. It is thought that this migration is mainly due to the selected (uniform) bottom friction value. The effects of the distribution of bottom friction values on constituents, elevations and currents outside the area of interest in this study, have not been analyzed. How bottom friction distributions and atmospheric forcing might lead to reduce uncertainties in the estimation of the tidal stream resource, is a subject of ongoing research.

3. Results and discussion

3.1. Model validation

Performance analysis of the implemented model was done for the complete year 2016, but here only results for winter and summer months are presented. As explained in Section 2.1, a set of sensitivity 1-month runs (July 2016) were performed to improve results by optimizing the bottom friction value. Here, the model is further validated for different time windows in 2016 at 13 locations, with different depths, along the Dutch coast. To compare the simulated time series of elevations with TG data, and identify potential seasonal effects caused by other forcing not included in our Thetis implementation, time windows of 2 months were defined to compute ABIAS, RMSD, NRMSD and CORR. A briefing of the validation results for all locations is presented in Table 1. At this stage, in the absence of current measurements, the performance analysis of the model is done only for sea surface elevations.

The model performance is verified first by comparing directly with the time-matched TGs data, which include the combined effects of atmospheric pressure changes, wind stress and surface waves. In panels a and b from Figs. 5 to 7, we present winter and summer time windows of 3 TG locations: Europlatform, Haringvliet10, and Q11. Here it is possible to observe how strong atmospheric forcing can be during winter months, with large differences between TGs and simulated time series and thus, the largest RMSD and NRMSD and lower CORR values. The occurrence of "events" where differences between modeled and measured elevations are largest, fall within the same days at different locations. For example, between February 1 to 4 (Figs. 5a to 7a), data from the ECMWF ERA5 atmospheric re-analyses [44] shows average wind intensities of 15.8 ms^{-1} and wave heights (combined swell and sea) of $\sim$ 4.5 m close to the Dutch coast. On the other hand, during summer months with mild winds and sea state conditions, the model

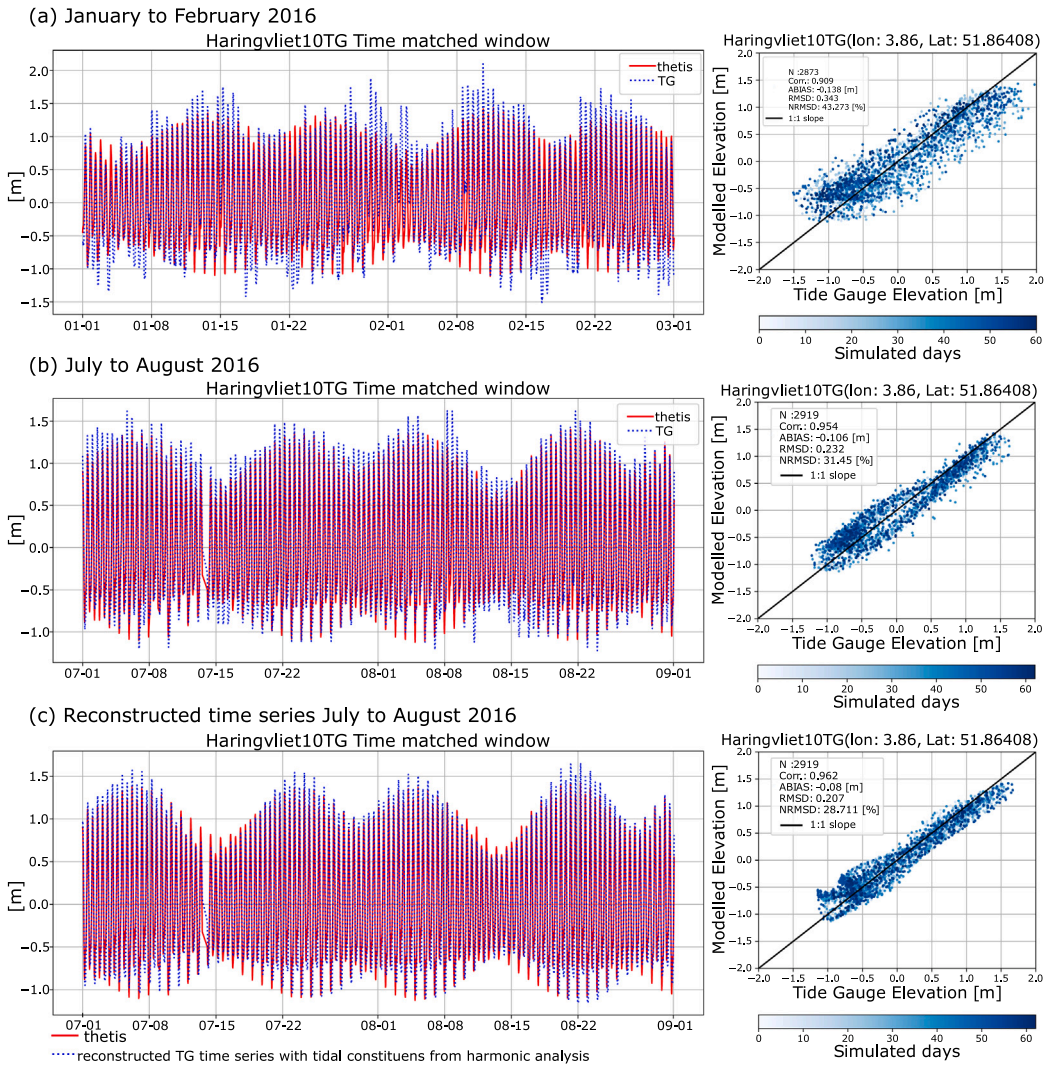

Fig. 6. Model performance briefing at Haringvliet10 TG. Analyzed time windows in year 2016: (a) January to February, (b) July to August, (c) July to August tide gauge reconstructed time series using tidal constituents only. In (b) and (c) there is a gap in the TG data between the 13 and 14 of July.

presents a closer behavior to the TGs' recorded data, with reductions > 15% in NRMSD compared to winter months, as well as higher correlations, typically over 0.93. This seasonal behavior is observed in all locations (see performance parameters for winter and summer months in Table 1).

Then, via harmonic analysis of each TG elevation time series with Uptide [45], the same tidal constituents used to force the model were computed at each location. Using the phase and amplitude of these tidal constituents, the time series of elevations caused only due to astronomical tide were reconstructed. In other words, this approach helps to filter out other forcing influences from the measurements, and allows to validate the model in terms of the effects of astronomical tides only, which is representative of the full year. In Figs. 5c, 6c and 7c it is already possible to observe how the simulations closely follow the elevation time series reconstructed only with tidal constituents, specially at Q11 (Fig. 7c). For all locations, NRMSD values are reduced about 4 % (sometimes 5 %) compared to the results obtained using the July-August data as recorded by the TGs (Table 1). Accuracy levels similar to those observed in Table 1, were obtained for the rest of the year, at each location, when the modeled elevation time series are compared with the TG data reconstructed using astronomical constituents only.

The overall high "model-TG" elevation correlations above 0.93 and reduced ABIAS proves a good representation of the tidal amplitudes along Dutch waters. There is already a noticeable reduction of the NRMSD for all locations when comparing model results with data as provided by the TGs in July-August. These values are specially low at Alte Weser and Terschelling Noordzee, with NRMSD of 16.6 and 17.69% respectively, when comparing with the TG time series reconstructed only with tidal constituents. It is also noticed that, in some places, the NRMSD can still be ~30 % even after filtering other forcing from the TG time series (in particular at Europlatform and Oosterschelde11; see Table 1). These differences are thought to be partially related to slight relative phase shifts between the modeled tidal wave and the TG data or other inaccuracies related to simplifications made in the model implementation (like homogeneous bottom friction and constant density). This effect could also be attributed to the mooring system of the instruments or inaccuracies in the phase values from the TPXO model constituents used along the boundary.

It is important to mention that the influence of other forcing over the sea surface elevations and currents profile should be further analyzed to assess its impact in the resource estimation. This is a subject of ongoing research and will be considered in a follow-up study.

3.2. Overview of current intensities

As seen in Fig. 8 mean and maximum current intensities due to astronomical tides do not have significant monthly variability, which is expected in a short term (≤ 1 year) analysis. Even though some

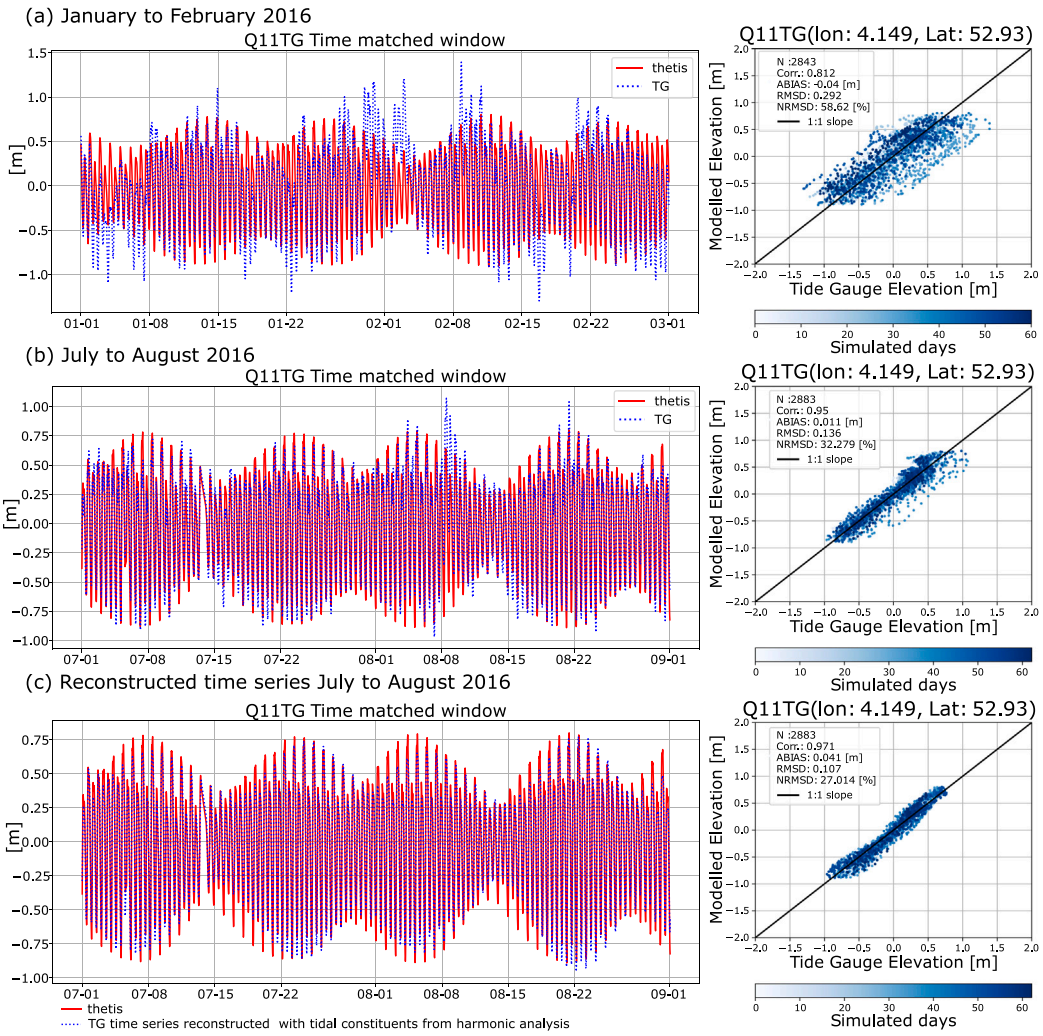

Fig. 7. Model performance briefing at Q11 TG. Analyzed time windows in year 2016: (a) January to February, (b) July to August, (c) July to August tide gauge reconstructed time series using tidal constituents only. In (b) and (c) there is a gap in the TG data on July 5, and between the 13 and 14 of July.

variability in tidal ranges would be detected in long term analyses, for example when the nodal tide (18.6 years cycle) is considered [46], its effect is thought to be insignificant in developed intensities compared to the influence of strong atmospheric events like storm surges. One month averaged current intensities of $\sim$ 0.4 to 0.6 m s^{-1} are found in long open beaches and in general at distances from the coast > 20 km. Sightly higher mean values are observed in the Westerschelde inlet. In Fig. 8b is possible to see that particularly high intensities are developed between the western Frisian islands, namely Texel, Vlieland and Terschelling.

Two different approaches are used to characterize the tidal stream. First, to have an idea of the spatial variability we defined 5 transects representative of the areas of interest mentioned above, and computed the intensities probability distribution function (PDF) at every point defined for each transect (Table 2). Then, as an attempt to characterize tidal stream resource availability per "zone", we computed the intensities PDF within 5 specific areas (Section 2.6). These are defined around the same locations as the transects, integrating the time series from each mesh node contained within the analyzed zone with depth >10 m. All computations are done over 2 months simulations.

The PDFs at the Westschelde transect show most frequent intensities of 0.8 and 0.7 m s^{-1} with a relative occurrence of ~15 % of the time. Intensities > 0.9 m s^{-1} are also developed, particularly for Westschelde-02 we found a cumulative occurrence of ~18 % for intensities >1.0 m s^{-1} (Fig. 9a). Although along the defined transect we predict, in average, a

Table 2
Transects used for intensities PDF construction. See locations in Appendix.

Location Name	Nodes	East [m]	North [m]	Depth [m]
Westerschelde	01	541443.54	5696811.99	21.4
	02	538114.46	5696674.65	24.5
	03	535709.64	5697117.84	26.5
	04	533061.45	5696953.62	18.6
Den Helder	01	618822.41	5871437.61	24.7
	02	615943.70	5870597.35	31.4
	03	614556.99	5869209.36	28.7
	04	612633.56	5867358.20	20.1
De Cocksdorp	01	625680.47	5893628.62	7.0
	02	624891.01	5894697.68	8.2
	03	623607.03	5895705.62	7.8
	04	620899.89	5895720.27	7.0
Oost Vlieland	01	645031.81	5908906.75	18.6
	02	642763.88	5909848.44	12.5
	03	639312.29	5910361.10	14.5
	04	637054.58	5912018.97	14.6
Hollum	01	675982.48	5921559.41	13.7
	02	673476.21	5923702.28	19.5
	03	671687.81	5925428.00	7.0
	04	669657.02	5928193.20	7.0

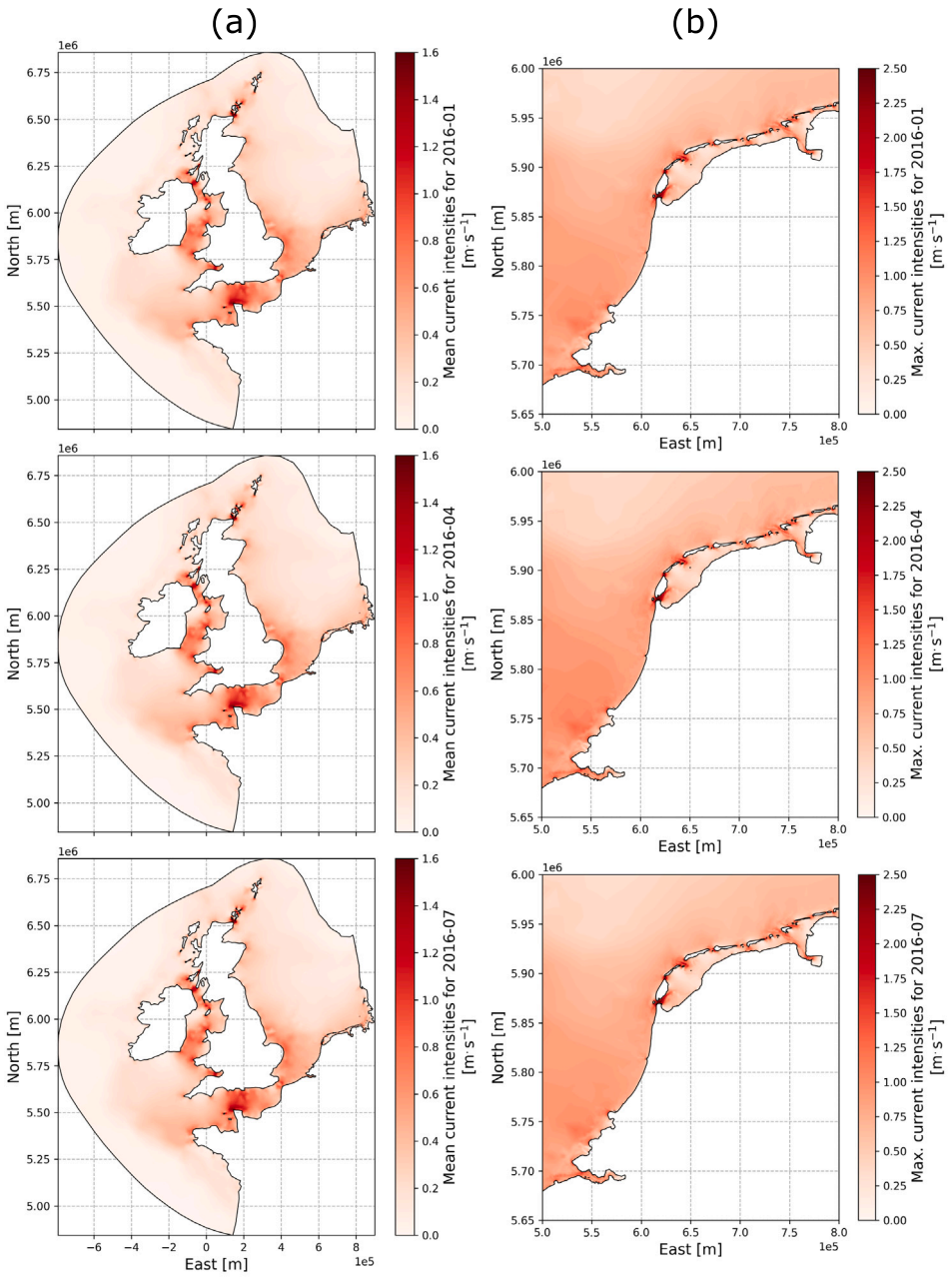

Fig. 8. (a) Mean current intensities from January, April and July 2016 for the complete modeled domain. (b) Detail of the maximum current intensities along the Dutch coast. Mean and maximum current intensities are computed from the time series of each mesh node.

cumulative occurrence of intensities ≥0.8 m s^{-1} close to 30 %, we note that this is a local behavior which could be attributed to bathymetric effects. When analyzing the complete area the overall occurrences peak drops to 0.6 m s^{-1} while the cumulative occurrences distribution shows that 50 % of the time the current intensities are smaller than 0.5 m s^{-1} (Fig. 10a). Even though no signs of model instabilities were detected within the analyzed area, these local higher values along the analyzed transect should be further verified with in-situ measurements.

Most promising results are found along the Den Helder transect, where the PDFs of the nodes placed between Texel and Den Helder (01,02,03) show a less pronounced peak of occurrences (~9 %) for intensities of 1.6 m s^{-1}, and where over 45 % of the time estimated current intensities are ≥1.0 m s^{-1} (Fig. 9b). For the complete area, the cumulative occurrences curve shows that 50 % of the time intensities are ≥0.6 m s^{-1} and 30 % of the time ≥0.9 m s^{-1}. In this case the lower intensities values (0.4 m s^{-1}) at the peak of occurrences in the PDF (10 %) are due to the contribution of the mesh nodes located offshore and away the passage between mainland and Texel, but notice that the occurrences differences between the peak and the intensities range 0.6 to 1.1 m s^{-1} are only about 2 % (Fig. 10b).

Although current intensities ≥1.1 m s^{-1} are predicted at De Cocksdorp transect, the depths of the analyzed locations are < 10 m and even reach the minimum depth of 7 m imposed for numerical reasons (Fig. 9c). Results for the full area, considering depths ≥ 10 m show that almost all of the selected mesh nodes are placed offshore, where about 40 % of the time current intensities are ≤0.3 m s^{-1} and with maximum values of ~0.9 m s^{-1} (Fig. 10c). The Hollum area present similar low intensities characteristics (Figs. 9e and 11b).

After the Den Helder area, the second location with higher simulated current intensities is Oost Vlieland, although larger variability in the position of the occurrences peak is observed between nodes. Intensities ≥1.2 m s^{-1} are predicted at nodes 01 and 02, which are placed

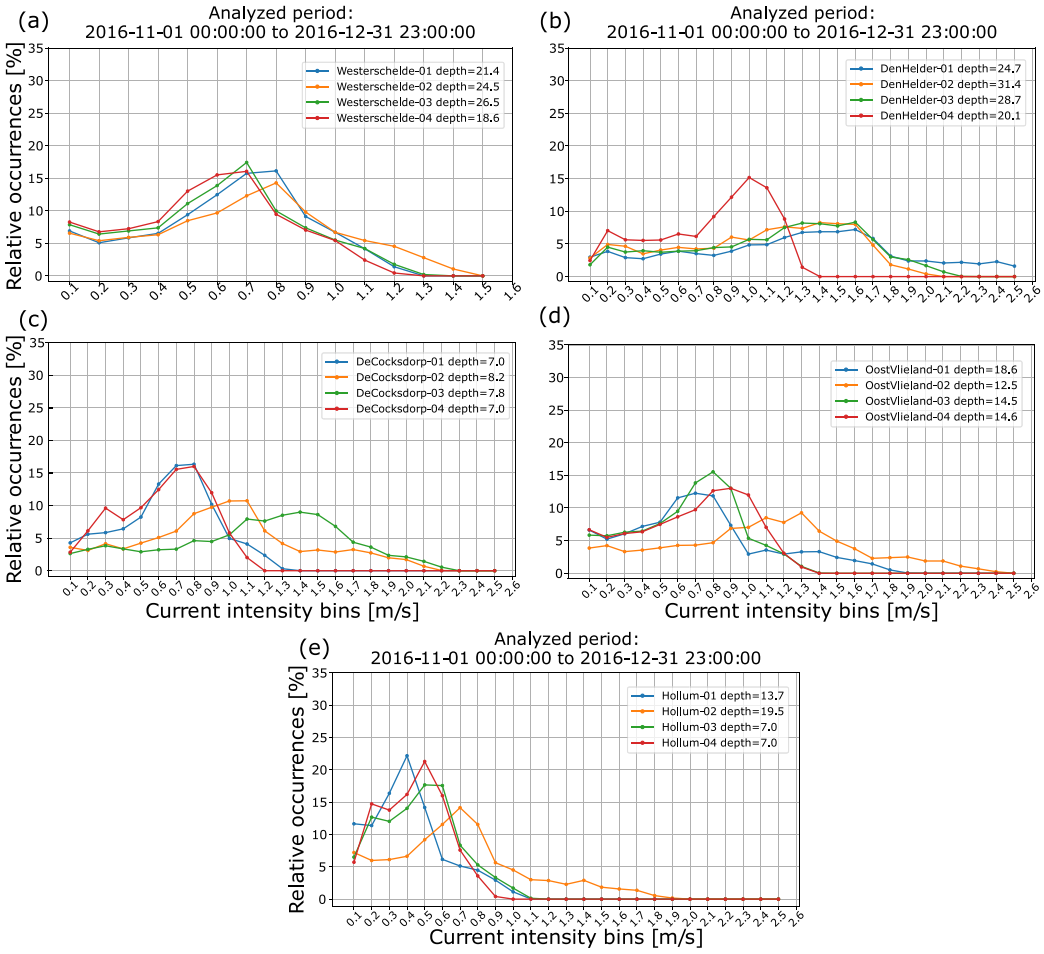

Fig. 9. Intensities PDF computed along transects at (a) Westschelde, (b) Den Helder, (c) De Cocksdorp, (d) Oost Vlieland and (e) Hollum. Relative occurrences normalized by the total amount of analyzed data at each transect node. Intensities bin width is 0.1 m s^{-1}. Specified nodes' depth is in meters with respect to the local mean sea level.

between Vlieland and Terchellig. Particularly for node Oost Vlieland-02 we estimate intensities ≥1.1 m s^{-1} over 45 % of the time (Fig. 9d). These high current locations are though to be local and probably nodes 03 and 04 are more representative of the full area conditions where we estimate that in average ~40 % of the time currents are ≥0.6 m s^{-1} with maximum intensities of ~1.5 m s^{-1} (Fig. 11b).

3.3. Tidal stream power density characterization

With a similar approach taken in Section 3.2, here we present an overview of the tidal stream power density. First, with a general look at mean and maximum W m^{-2} along the Dutch coast, and then with a more detailed view on those identified locations with higher current intensities that could be suitable for deployment of tidal energy converters (TEC).

In Fig. 12 we present the maximum and mean tidal power density for December 2016. As shown in Section 3.2, current intensities estimated from astronomical tides only do not vary significantly along the year (Fig. 8). This was verified by computing the differences between each month intensities mean with respect to the 1-year mean which showed negligible variations (≤ 0.01 m s^{-1}) in only localized areas (not shown). Thus, the maximum and mean power density computed for December 2016 are considered representative of the full year.

From the general results in Fig. 12 is already noticed that even though there are maximum power density values of about 1 kW m^{-2} within the Westschelde area, the mean shows considerable lower values of ~0.3 kW m^{-2} in the most energetic areas (see Fig. 13a). Similar conditions are found at Oost vlieland and Hollum (Fig. 14). In these latter locations it was already expected given the lower current intensities developed (particularly at Hollum), and most frequent speeds concentrated between 0.4 and 0.5 m s^{-1} (Fig. 11).

Den Helder presents the highest power density from the analyzed locations, with areas reaching values > 10 kW m^{-2} (Fig. 13b). Additionally, it also presents the largest mean tidal power density (up to ~ 3 kW m^{-2}), which is not only related to the development of higher current intensities, but also due to the more even intensities' distribution (or absence of a dominant occurrences peak; Fig. 9b and 10b). We found similar high mean power density conditions at De Cocksdorp, but as mentioned in Section 3.2 shallow depths in this location may represent a problem for TEC operation.

3.4. Power density estimations in adjusted areas

Using the complete 1-year tide database generated and the same transects described in Table 2 we computed the power density distributions using a bin width of 200 W m^{-2} (Fig. 15). In this case, the transect at Hollum is not included since this area does not present interesting stream conditions. Analog to the current intensities PDF generated per area in Figs. 10 and 11, power density PDFs were generated considering the contribution of all mesh nodes with depth larger than 10 m within a specific zone. Nodes' selection was done using an adjusted area, which was defined taking into account the spatial distribution of higher mean values observed in Figs. 13 and 14. The PDF curves were computed using tidal power density bins of 100 W m^{-2}, and only for the areas considered to have the higher potential for energy extraction, Den Helder and Oost Vlieland (Fig. 16). Note that in this selection land has

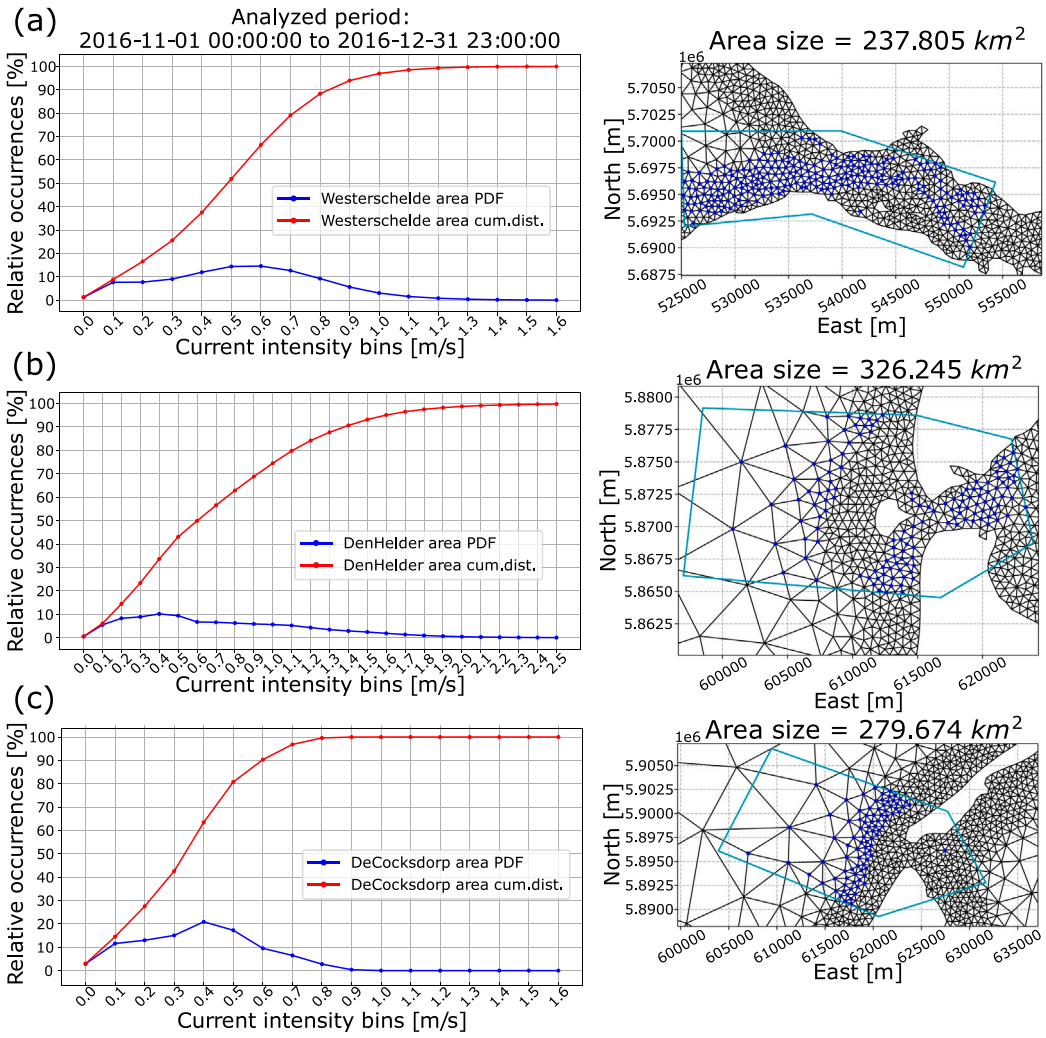

Fig. 10. Intensities PDF computed at different areas: (a) Westschelde, (b) Den Helder, (c) De Cocksdorp. Mesh nodes in blue have an estimated depth > 10 m with respect to MSL. Relative occurrences normalized by the total amount of analyzed data with the contribution of all nodes in blue. Intensities bin width is 0.1 ms^{-1}. The area size corresponds to the one defined by the polygon in cyan. Offshore extension of polygons for (b) and (c) is ~20 km.

been excluded, in an attempt to have more direct relation between the analyzed areas and the power density PDFs.

In all defined transects the highest occurrences peak is located at 100 W m^{-2} (meaning in the [0-200] W m^{-2} range). This peak is specially high at the Westschelde transect reaching ~75 % in Westschelde-04. Along this transect the occurrences of higher power density drop significantly in all locations, with less than 30 % at Westschelde-01 and 02, and less than 20 % at Westschelde-03 and 04 at 300 W m^{-2}. It is estimated that ~26.5% of the time the stream power density is > 300 W m^{-2} at Westschelde-04, slightly higher occurrence at Westschelde-03, and ~47 % of the time at Westschelde-02. The latter location being the only one with occurrences of power density ≥900 W m^{-2} (Fig. 15a).

Along the Den Helder transect, locations 01 to 03 present power density occurrences that 70 % of the time are ≥ 300 W m^{-2} and in average 45 % of the time ≥ 900 W m^{-2}. Given the current intensities' characteristics at Den Helder-04 (see Fig. 9b), no power density occurrences ≥ 1300 W m^{-2} are estimated, but this location still presents 42 % of the occurrences concentrated between 500 to 1100 W m^{-2} (Fig. 15b).

At De Cocksdorp, locations 02 and 03 present the most interesting conditions of this transect, where we found stream power density values ≥ 500 W m^{-2} 51 % and 66 % of the time respectively. De Cocksdorp-01 and 04 locations present the minimum depth threshold imposed in the model, which is partly why these results should be revisited in future studies (Fig. 15c).

Finally, for Oost Vlieland at locations 01, 03 and 04 we found power density values ≥ 300 W m^{-2} 45 % of the time and more. Particularly, the highest values are found at Oost Vlieland-02 where 45 % of the time the power density obtained is ≥ 700 W m^{-2} and almost 40 % ≥ 900 W m^{-2} (Fig. 15d). These results confirm that Den Helder and Oost Vlieland are the areas with higher potential for energy extraction along the Dutch coast.

When considering the contribution of all selected nodes in the Den Helder area, in average 55 % of the time the power density is ≥ 300 W m^{-2} and only ~ 27 % of the time ≥ 900 W m^{-2} (Fig. 16a), which suggest that probably the most "energetic" locations are placed in the neighborhood of the previously analyzed transect. The Oost Vlieland area PDF (Fig. 16b) presents power density levels ≥ 300 W m^{-2} 30 % of the time, 15 % lower than in the locations along the transect previously analyzed and power density levels ≥ 900 W m^{-2} less than 10 % of the time, similar to locations 03 and 04 in the Oost Vlieland transect (Fig. 15d). With these results, it is expected that the higher power density levels of this area are found in the surroundings of location Oost Vlieland-02.

4. Conclusions

In the preset document, we have developed the first tidal stream assessment for Dutch waters, using a high resolution tide model specially adjusted and validated for this purpose. The main objective of this

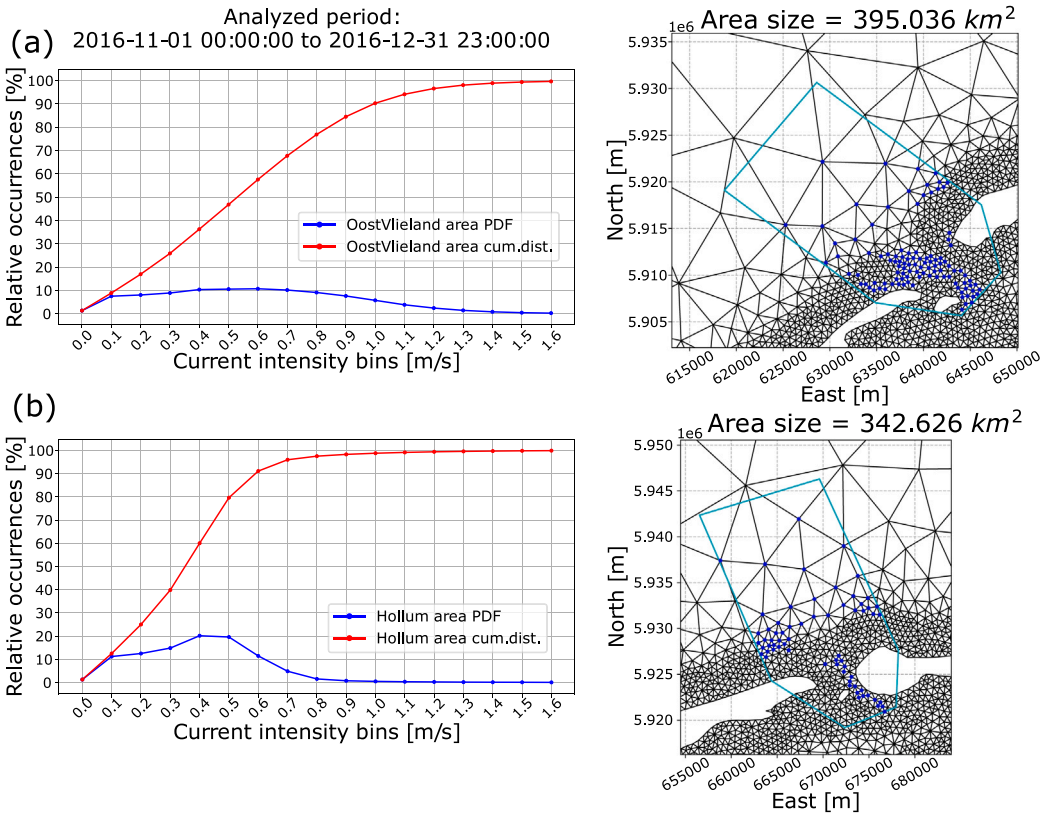

Fig. 11. Intensities PDF computed at different areas: (a) Oost Vlieland and (b) Hollum. Mesh nodes in blue have an estimated depth > 10 m with respect to MSL. Relative occurrences normalized by the total amount of analyzed data with the contribution of all nodes in blue. Intensities bin width is 0.1 m s^{-1}. The area size corresponds to the one defined by the polygon in cyan. Offshore extension of polygons is ~20 km.

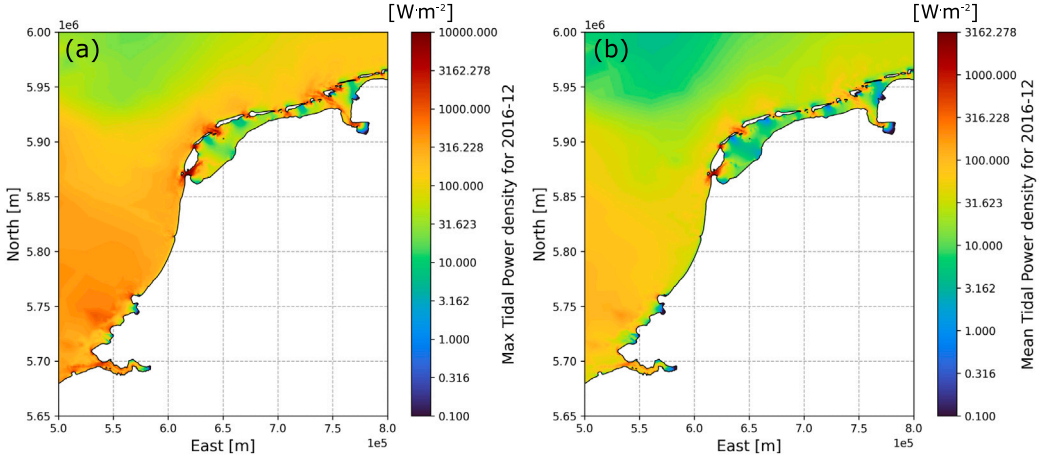

Fig. 12. (a) Maximum and (b) mean tidal power density along the Dutch coast computed for December 2016.

study was to characterize and identify areas with potential for energy extraction along the coast of The Netherlands. To perform the tidal stream characterization, a 1 year database of currents and elevations was generated, and an area based analysis, including depth restrictions, was proposed.

The implemented hydrodynamic model (Thetis), with resolution of 500 m within the first 4 km from the coast, was validated using sea surface elevations from tide gauges at 13 location along the Dutch coast. When comparing with time series reconstructed using tidal harmonics only, the model showed high correlation levels (typically > 0.95), and reduce amplitude bias range between −0.14 and −0.01 m. These results were verified to be consistent throughout the full modeled year. Direct comparison with the measured time series for winter months (January-February) lead to lower correlation values between 0.83 and 0.9 with larger biases and errors. This is due to the effect of atmospheric forcing that was not considered in the simulations. The clear presence of non-astronomical forcing during winter months can have non negligible effect on the velocities profile.

Based on an overview of tidal characteristics along the Dutch coast, the following the locations were initially selected as potential sites for stream energy conversion: Westerschelde, Den Helder, De Cocksdorp, Oost Vlieland and Hollum. Then, following the method proposed, the description of these areas was done using the intensities probability distribution function (PDF). The analyzed transects showed local "hot

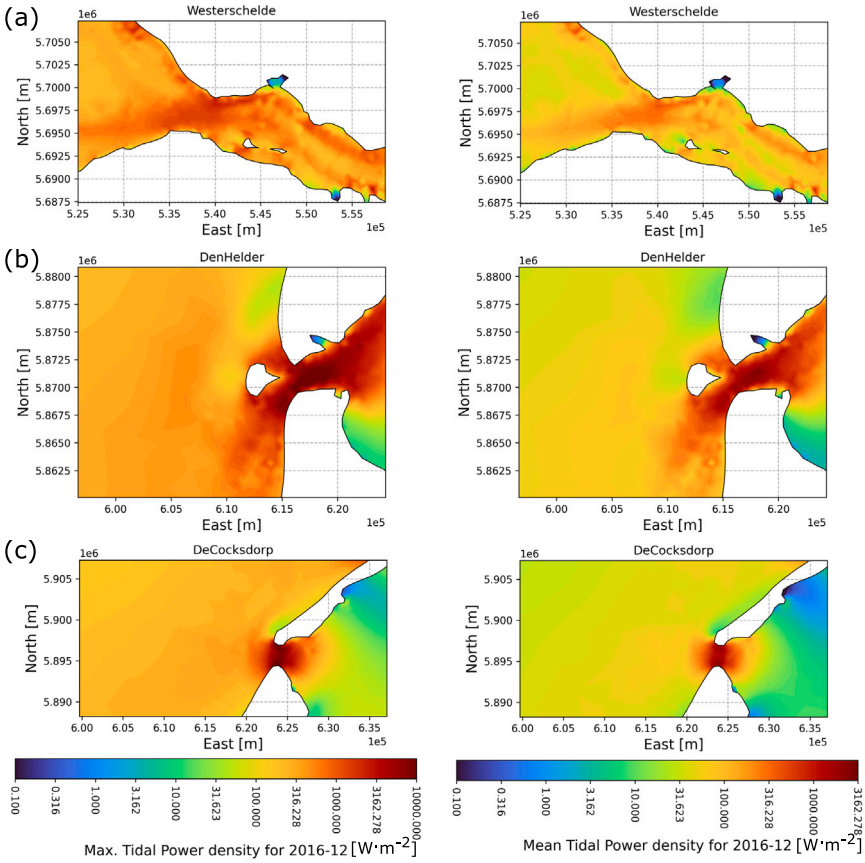

Fig. 13. Maximum and mean tidal power density at (a) Westschelde, (b) Den Helder and (c) De Cocksdorp. Results from December 2016 simulation.

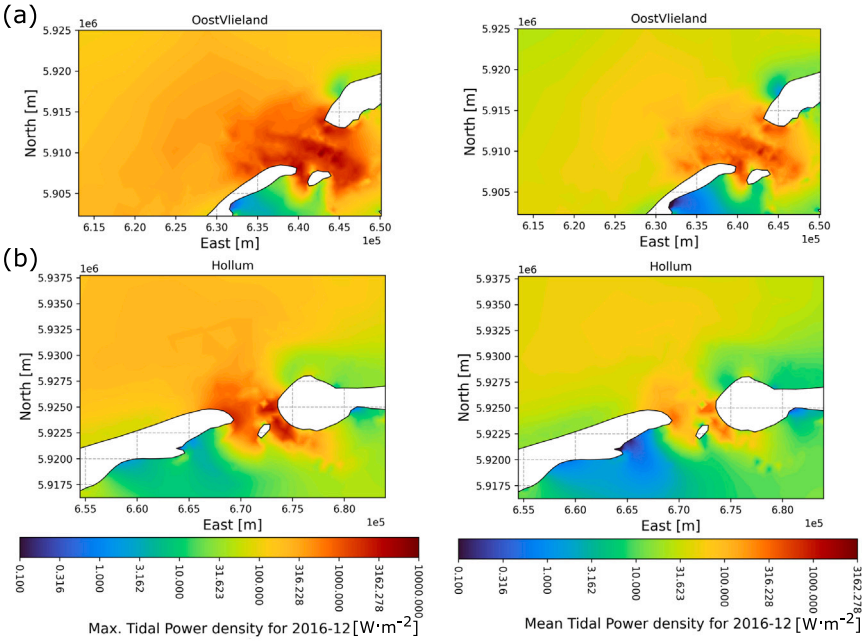

Fig. 14. Maximum and mean tidal power density at (a) Oost Vlieland and (b) Hollum. Results from December 2016 simulation.

spots" in Den Helder and Oost Vlieland, where current intensities >1.0 m s^{-1} (and also >1.5 m s^{-1}) were estimated. Other locations like De Cocksdorp showed interesting current conditions, but depths in the area might represent a problem for TEC operation. The estimation of the currents' PDF per area also showed high occurrences of intensities ≥0.6 m s^{-1}, over 40 % and 50 % of the time at Oost Vlieland and Den Helder respectively.

Den Helder presented the highest current intensities with also high occurrences in time. At particular locations, over 45 % of the time the estimated intensities are ≥1.0 m s^{-1}. When the analysis is performed

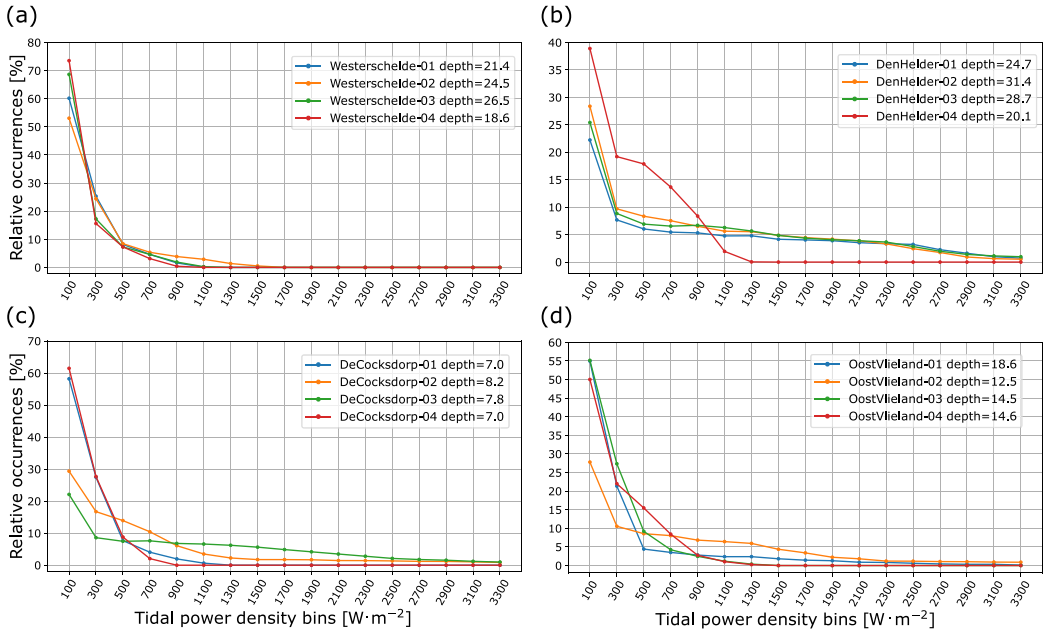

Fig. 15. Tidal stream power density distributions at (a) Westschelde, (b) Den Helder, (c) De Cocksdorp and (d) Oost Vlieland transects. Results computed with full year 2016 simulation. Power density bins width is 200 W m^{-2}. Transects' locations specified in Table 2.

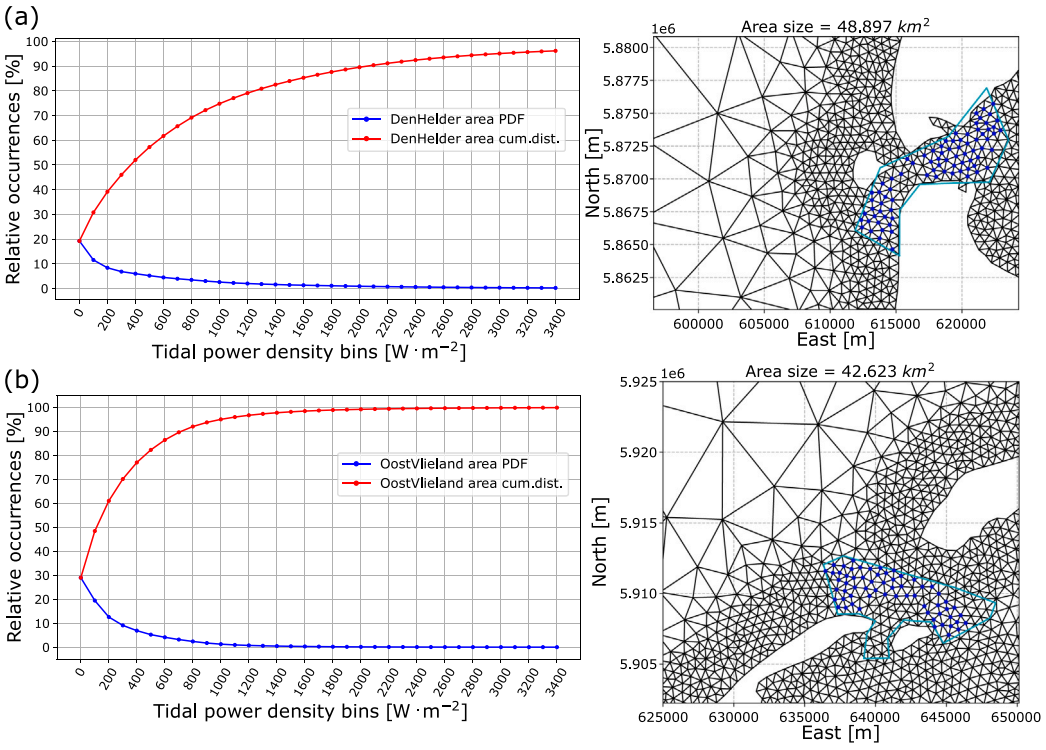

Fig. 16. Tidal stream power density distributions at (a) Den Helder and (b) Oost Vlieland areas. Results computed with full year 2016 simulation. Power density bins width is 100 W m^{-2}. The area size corresponds to the one defined by the polygon in cyan. In blue, mesh nodes with depth > 10 m.

over this area, the cumulative occurrences curve shows that in average 50 % of the time intensities are ≥0.6 m s^{-1} and 30 % of the time ≥0.9 m s^{-1}. From the current's intensities point of view, this is considered to be the location with higher potential for tidal stream energy extraction.

Given their currents' characteristics, the stream power density analysis was only centered on Den Helder and Oost Vlieland considering an adjusted area. The estimated power density is 55 % of the time ≥ 300 W m^{-2} and about 27 % of the time ≥ 900 W m^{-2} at Den Helder, and 30 % of the time ≥ 300 W m^{-2} and less than 10 % of the time ≥ 900 W m^{-2} at Oost Vlieland. These results are sensitive to the area defined to construct the power density PDFs at each location, which is the main downside of the proposed analysis method. Nevertheless, it is considered that the suggested areas are representative of the zones with significant potential for energy extraction. Occurrences of the highest power density levels were found along the defined transects at these locations, which suggests that the most energetic sectors are highly localized.

Fig. A.17. Selected locations at (a) Den Helder and (b) De Cocksdorp areas. Map data are taken from ©Google Landsat/Copernicus.

In general the tidal resource of the Netherlands is classified as low density, therefore, the adaptation/development of turbines for low tidal stream and/or reduced depth areas is a vital step to make the use of the available resource feasible. It is expected that current tidal stream devices with large diameters (e.g.; 18 m of Meygen) will not be as effective in production. Therefore, we anticipate that the re-scaling of the design according to the local tidal resource will lead to significantly lower rotor diameter, and much smaller installed capacities. From the obtained results and analyzed depths, our first estimates indicate that a rotor diameter of 5 m achieves a much higher capacity factor than a larger diameter, and hence a smaller installed capacity turbine.

It is expected that adding atmospheric pressure forcing and/or the coupling with a wave model, the simulations of seasonal changes in the time series of elevations, and flows can be improved significantly. The influence of atmospheric forcing on the estimations of the stream resource should be further analyzed in future studies. On the same line, the spatially homogeneous bottom friction value defined after a sensitivity analysis helped to reduce tidal amplitude errors in most analyzed TG locations, but it can also introduce spurious results elsewhere. Given the cumulative effect of the bottom friction, it is expected that a more detailed representation, considering spatial changes related to bottom sediment types, will also help to improve the accuracy of the simulated levels and velocities. The minimum depth threshold applied for the simulations, could affect the accuracy of the results obtained in very shallow areas and particularly in the Wadden Sea. Finally, calibration and validation of the implemented model was done only against time series of elevations. Even though an overall reduced amplitudes' bias and high correlation values were obtained, this does not necessarily extrapolate to the simulated velocity components (u and v), specially in areas with intricate bathymetry features. These elements and their effect in the stream power density estimations are topics of further research.

We note that this is the first high resolution Dutch tidal stream assessment, with main focus on examining the underlying resource characteristics (intensities, distributions, locations). No electrical aspects nor alternatives of tidal stream extraction devices have been considered in this study. Both elements are of great importance in the design of an extraction array and by extent, the estimation of the installed capacity or production estimates. These aspects, and grid connection alternatives are subjects of future studies.

CRediT authorship contribution statement

Matias Alday: Conceptualization, Methodology and proposed analysis, Software implementation, Data curation, Writing (original draft preparation and corrections). **George Lavidas:** Conceptualization, Methodology, Revision and editing, Funding acquisition.

Declaration of competing interest

The authors declare that they have no known competing financial interests or personal relationships that could have appeared to influence the work reported in this paper.

Data availability

Please contact MA (M.F.AldayGonzalez@tudelft.nl) or GL (G.Lavidas@tudelft.nl) to get access.

Acknowledgments

The authors would like to thank Tuomas Karna, Jon Hill and Joe Wallwork for their continuous help on the implementation of Thetis, mesh generation and constructive discussions. Special thanks to Dennis Palagin who made it possible to install Thetis in the DelftBlue HPC and to Athanasios Angeloudis who went through the document on its early stage and provided important insights to improve its content. Finally, we would like to thank the anonymous reviewers who provided valuable comments and suggestions to give this study its final shape.

This work was part of the Dutch-Wave And Tidal Energy ResourceS (Dutch-WATERS) project which received funding from TKI Delta Technology (Deltatechnologie), supported by the Ministry of Economic Affairs and Climate Policy, The Netherlands.

Appendix. Transects locations for current and power density characterization

The following figures show the location of the transects defined in Section 3.2 for the analysis of current intensities and power density distribution (see Figs. A.17–A.19).

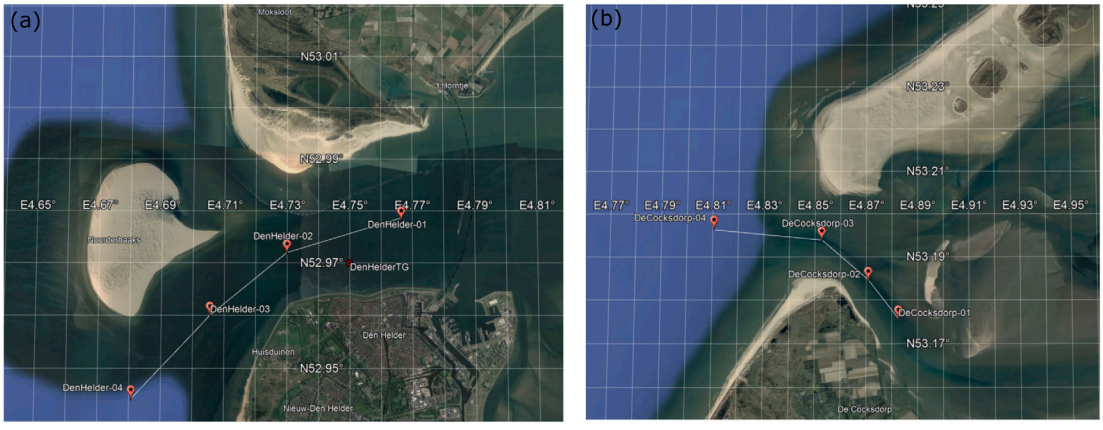

Fig. A.18. Selected locations at (a) Den Helder and (b) De Cocksdorp areas. Map data are taken from ©Google Landsat/Copernicus.

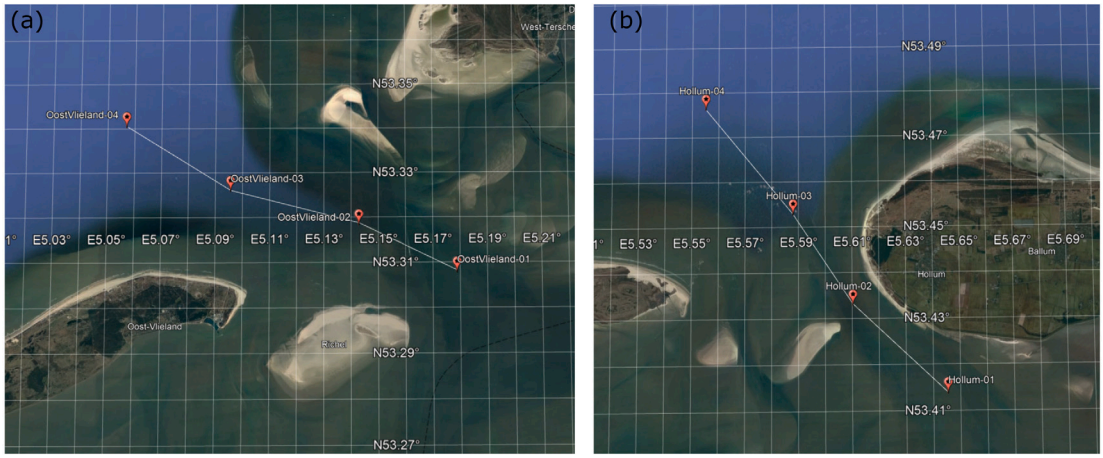

Fig. A.19. Selected locations at (a) Oost Vlieland and (b) Hollum areas. Map data are taken from ©Google Landsat/Copernicus.

References

[1] S.P. Neill, M.R. Hashemi, M.J. Lewis, Tidal energy leasing and tidal phasing, Renew. Energy 85 (2016) 580–587.

[2] S.P. Neill, M. Hemer, P.E. Robins, A. Griffiths, A. Furnish, A. Angeloudis, Tidal range resource of Australia, Renew. Energy 170 (2021) 683–692.

[3] C.R. Vogel, D.T. Taira, B.S. Carmo, G.R.d.S. Assi, R.H. Willden, J.R. Meneghini, Prospects for tidal stream energy in the UK and South America: A review of challenges and opportunities, Polytechnica 2 (1) (2019) 97–109.

[4] C.J. Mejia-Olivares, I.D. Haigh, N.C. Wells, D.S. Coles, M.J. Lewis, S.P. Neill, Tidal-stream energy resource characterization for the Gulf of California, México, Energy 156 (2018) 481–491.

[5] N. Guillou, S.P. Neill, P.E. Robins, Characterising the tidal stream power resource around France using a high-resolution harmonic database, Renew. Energy 123 (2018) 706–718.

[6] M. Guerra, R. Cienfuegos, J. Thomson, L. Suarez, Tidal energy resource characterization in Chacao Channel, Chile, Int. J. Mar. Energy 20 (2017) 1–16.

[7] K. Orhan, R. Mayerle, W.W. Pandoe, Assesment of energy production potential from tidal stream currents in Indonesia, Energy Procedia 76 (2015) 7–16.

[8] R. Burrows, N. Yates, T. Hedges, M. Li, J. Zhou, D. Chen, I. Walkington, J. Wolf, J. Holt, R. Proctor, Tidal energy potential in UK waters, in: Proceedings of the Institution of Civil Engineers-Maritime Engineering, Vol. 162, No. 4, Thomas Telford Ltd, 2009, pp. 155–164.

[9] J. Frau, Tidal energy: promising projects: La Rance, a successful industrial-scale experiment, IEEE Trans. Energy Convers. 8 (3) (1993) 552–558, http://dx.doi.org/10.1109/60.257073.

[10] M.C. Easton, D.K. Woolf, P.A. Bowyer, The dynamics of an energetic tidal channel, the Pentland Firth, Scotland, Cont. Shelf Res. 48 (2012) 50–60.

[11] L. Shah, P. De Boer, Ebb-Tidal Delta Deposits Along the West Frisian Islands (The Netherlands): Processes, Facies Architecture and Preservation, CSPG Special Publications, 1991.

[12] L. Sha, J. Van den Berg, Variation in ebb-tidal delta geometry along the coast of the Netherlands and the German Bight, J. Coast. Res. (1993) 730–746.

[13] D. Wesselman, R. de Winter, A. Engelstad, R. McCall, A. van Dongeren, P. Hoekstra, A. Oost, M. van der Vegt, The effect of tides and storms on the sediment transport across a Dutch barrier island, Earth Surf. Process. Landf. 43 (3) (2018) 579–592.

[14] H.E. Pelling, J.M. Green, S.L. Ward, Modelling tides and sea-level rise: To flood or not to flood, Ocean Model. 63 (2013) 21–29.

[15] L. Jiang, T. Gerkema, D. Idier, A. Slangen, K. Soetaert, Effects of sea-level rise on tides and sediment dynamics in a Dutch tidal bay, Ocean Sci. 16 (2) (2020) 307–321.

[16] R. Kastelein, N. Jennings, M. Scholl, M. Leopold, R. Kastelein, Position Paper: Effects of the Eastern Scheldt Storm Surge Barrier and Tidal Energy Turbines on Harbor Porpoise (*Phocoena phocoena*) and Harbor Seal (*Phoca vitulina*) Movements SEAMARCO Report 2019-01 February 2019, Technical Report, SEAMARCO, 2019.

[17] A. de Fockert, A.C. Bijlsma, T.S. O'Mahoney, W. Verbruggen, P.C. Scheijgrond, Z.B. Wang, Assessment of the impact of tidal power extraction from the eastern scheldt storm surge barrier through the evaluation of a pilot plant, Renew. Energy 213 (2023) 109–120, http://dx.doi.org/10.1016/j.renene.2023.06.001, URL https://www.sciencedirect.com/science/article/pii/S0960148123007711.

[18] H. Díaz, C.G. Soares, Review of the current status, technology and future trends of offshore wind farms, Ocean Eng. 209 (2020) 107381, http://dx.doi.org/10.1016/j.oceaneng.2020.107381.

[19] N. Akbari, D. Jones, R. Treloar, A cross-European efficiency assessment of offshore wind farms: A DEA approach, Renew. Energy 151 (2020) 1186–1195, http://dx.doi.org/10.1016/j.renene.2019.11.130.

[20] N.A. Steins, J.A. Veraart, J.E. Klostermann, M. Poelman, Combining offshore wind farms, nature conservation and seafood: Lessons from a Dutch community of practice, Mar. Policy 126 (2021) 104371, http://dx.doi.org/10.1016/j.marpol.2020.104371.

[21] G.D. Egbert, S.Y. Erofeeva, Efficient inverse modeling of barotropic ocean tides, J. Atmos. Ocean. Technol. 19 (2) (2002) 183–204, http://dx.doi.org/10.1175/1520-0426(2002)019<0183:EIMOBO>2.0.CO;2.

[22] L. Pineau-Guillou, PREVIMER. Validation des atlas de composantes harmoniques de hauteurs et courants de marée, Technical Report, Ifremer ODE/DYNECO/PHYSED, 2013, URL https://archimer.ifremer.fr/doc/00157/26801/.

[23] L. Carrere, F. Lyard, M. Cancet, A. Guillot, FES 2014, a new tidal model on the global ocean with enhanced accuracy in shallow seas and in the arctic region, in: EGU General Assembly Conference Abstracts, 2015, p. 5481.

[24] D.M. Ingram, Protocols for the Equitable Assessment of Marine Energy Converters, Lulu. com, 2011.

[25] T. Kärnä, S.C. Kramer, L. Mitchell, D.A. Ham, M.D. Piggott, A.M. Baptista, Thetis coastal ocean model: discontinuous Galerkin discretization for the three-dimensional hydrostatic equations, Geosci. Model Dev. 11 (11) (2018) 4359–4382, http://dx.doi.org/10.5194/gmd-11-4359-2018, URL https://gmd.copernicus.org/articles/11/4359/2018/.

[26] F. Rathgeber, D.A. Ham, L. Mitchell, M. Lange, F. Luporini, A.T. McRae, G.T. Bercea, G.R. Markall, P.H. Kelly, Firedrake: automating the finite element method by composing abstractions, ACM Trans. Math. Softw. 43 (3) (2016) 1–27.

[27] S. Balay, W.D. Gropp, L.C. McInnes, B.F. Smith, Efficient management of parallelism in object oriented numerical software libraries, in: E. Arge, A.M. Bruaset, H.P. Langtangen (Eds.), Modern Software Tools in Scientific Computing, Birkhäuser Press, 1997, pp. 163–202.

[28] S. Balay, S. Abhyankar, M.F. Adams, S. Benson, J. Brown, P. Brune, K. Buschelman, E. Constantinescu, L. Dalcin, A. Dener, V. Eijkhout, W.D. Gropp, V. Hapla, T. Isaac, P. Jolivet, D. Karpeev, D. Kaushik, M.G. Knepley, F. Kong, S. Kruger, D.A. May, L.C. McInnes, R.T. Mills, L. Mitchell, T. Munson, J.E. Roman, K. Rupp, P. Sanan, J. Sarich, B.F. Smith, S. Zampini, H. Zhang, H. Zhang, J. Zhang, PETSc/TAO Users Manual, Technical Report ANL-21/39 - Revision 3.17, Argonne National Laboratory, 2022.

[29] M.R. Hestenes, E. Stiefel, Methods of conjugate gradients for solving, J. Res. Natl. Bur. Stand. 49 (6) (1952) 409.

[30] U.M. Ascher, S.J. Ruuth, B.T.R. Wetton, Implicit-explicit methods for time-dependent partial differential equations, SIAM J. Numer. Anal. 32 (3) (1995) 797–823, http://dx.doi.org/10.1137/0732037.

[31] R. Courant, On the partial difference equations of mathematical physics, Math. Ann. 100 (1928) 32–74.

[32] T. Kärnä, J.G. Wallwork, S.C. Kramer, Adjoint-based optimization of a regional water elevation model, 2022, arXiv preprint arXiv:2205.01343.

[33] A. Avdis, A.S. Candy, J. Hill, S.C. Kramer, M.D. Piggott, Efficient unstructured mesh generation for marine renewable energy applications, Renew. Energy 116 (2018) 842–856.

[34] P. Mooney, M. Minghini, et al., A Review of Openstreetmap Data, Ubiquity Press, 2017.

[35] S. Thierry, S. Dick, S. George, L. Benoit, P. Cyrille, EMODnet bathymetry a compilation of bathymetric data in the European waters, in: OCEANS 2019-Marseille, IEEE, 2019, pp. 1–7.

[36] J. Lambrechts, R. Comblen, V. Legat, C. Geuzaine, J.-F. Remacle, Multiscale mesh generation on the sphere, Ocean Dyn. 58 (5) (2008) 461–473.

[37] CMEMS, Copernicus Marine In Situ Tac Data Management Team, Product User Manual for multiparameter Copernicus In Situ TAC (PUM), Report (Technical Document (Specification, Manual)), Copernicus Marine environment monitoring service, 2021, http://dx.doi.org/10.13155/43494.

[38] J.M. Huthnance, Physical oceanography of the North Sea, Ocean Shorel. Manag. 16 (3–4) (1991) 199–231.

[39] G.I. Taylor, Tidal oscillations in gulfs and rectangular basins, Proc. Lond. Math. Soc. 2 (1) (1922) 148–181.

[40] J. Proudman, A.T. Doodson, V. The principal constituent of the tides of the North Sea, Philos. Trans. R. Soc. Lond. Ser. A 224 (616–625) (1924) 185–219.

[41] P.C. Roos, J.J. Velema, S.J. Hulscher, A. Stolk, An idealized model of tidal dynamics in the North Sea: resonance properties and response to large-scale changes, Ocean Dyn. 61 (12) (2011) 2019–2035.

[42] M. Quante, F. Colijn, North Sea Region Climate Change Assessment, Springer Nature, 2016.

[43] L. Jänicke, A. Ebener, S. Dangendorf, A. Arns, M. Schindelegger, S. Niehüser, I.D. Haigh, P. Woodworth, J. Jensen, Assessment of tidal range changes in the North Sea from 1958 to 2014, J. Geophys. Res.: Oceans 126 (1) (2021) e2020JC016456.

[44] H. Hersbach, B. Bell, P. Berrisford, S. Hirahara, A. Horányi, J. Muñoz-Sabater, J. Nicolas, C. Peubey, R. Radu, D. Schepers, A. Simmons, C. Soci, S. Abdalla, X. Abellan, G. Balsamo, P. Bechtold, G. Biavati, J. Bidlot, M. Bonavita, G.D. Chiara, P. Dahlgren, D. Dee, M. Diamantakis, R. Dragani, J. Flemming, R. Forbes, M. Fuentes, A. Geer, L. Haimberger, S. Healy, R.J. Hogan, E. Hólm, M. Janisková, S. Keeley, P. Laloyaux, P. Lopez, C. Lupu, G. Radnoti, P. de Rosnay, I. Rozum, F. Vamborg, S. Villaume, J.-N. Thépaut, The ERA5 global reanalysis, Q. J. R. Meteorol. Soc. 146 (2020) 1999–2049, http://dx.doi.org/10.1002/qj.3803.

[45] S. Kramer, T. Kärnä, J. Hill, S. Funke, Uptide: First release of uptide v1.0, 2020, URL https://github.com/stephankramer/uptide.

[46] R. Hagen, A. Plüß, L. Jänicke, J. Freund, J. Jensen, F. Kösters, A combined modeling and measurement approach to assess the nodal tide modulation in the North Sea, J. Geophys. Res.: Oceans 126 (3) (2021) e2020JC016364.